Supplemental File for

Epigenetic drift score captures directional methylation variability and links aging to transcriptional, metabolic, and genetic alterations

Xiu Fan, Qili Qian, Wenran Li, Tianzi Liu, Changqing Zeng, Peilin Jia, Huandong Lin, Xin Gao, Li Jin, Mingfeng Xia, Sijia Wang, Fan Liu

Table of Contents

Supplemental Notes

Study Cohorts, Data Provenance, and Ethics Statement

NSPT, CAS, and Changfeng cohorts have been established by our group and described previously. All DNA methylation data analyzed in this study were obtained from publicly accessible databases from previously published studies. Written informed consent was obtained from all participants as part of the original studies, and each original study was approved by the respective institutional review board. Detailed descriptions of the cohorts are as follows:

National Survey of Physical Traits cohort (NSPT)

The NSPT cohort has been previously described in (Peng et al. 2024). This cohort consists of 3,538 Chinese individuals (mean age 50.2 years, 37.0% male). The original study was approved by the Ethics Committee of Human Genetic Resources of the School of Life Sciences, Fudan University, Shanghai (14117). Data are available at the National Omics Data Encyclopedia (NODE, https://www.biosino.org/node) under accession number OEZ00008120.

Chinese Academy of Sciences cohort (CAS)

The CAS cohort has been described in (Peng et al. 2024). This replication cohort includes 1,060 individuals, predominantly highly educated individuals in intellectual professions (mean age 40.8 years, 59.7% male). The original study was approved by the Institutional Review Board of Beijing Institute of Genomics and Zhongguancun Hospital (2020H020,

2021H001, and 20201229). The data are available at OMIX (https://ngdc.cncb.ac.cn/omix/) under accession code OMIX004333.

Shanghai Changfeng cohort (Changfeng)

The Changfeng cohort is a longitudinal study previously described in (Gao et al. 2010; Li et al. 2024). The dataset includes 407 subjects with a median follow-up of 4 years. The original study was approved by the Research Ethics Committee of Zhongshan Hospital, Fudan University (No. 2008-119 and B2013-132). Data are available at NODE (https://www.biosino.org/node) under accession number OEP00004768.

Genome-wide DNA Methylation Profiling and Quality Control

The methods for DNA extraction, bisulfite conversion, and genome-wide DNA methylation profiling using the Illumina MethylationEPIC BeadChip for all three cohorts (NSPT, CAS, and Changfeng) were detailed in their original publications (Li et al. 2024; Peng et al. 2024).

For the present study, we obtained the raw data and performed the following quality control and processing steps. Raw .idat files were processed using minfi (for NSPT) or ChAMP (for CAS and Changfeng) (Aryee et al. 2014; Morris et al. 2014). Quality control excluded samples with unclear gender and probes with SNPs, sex chromosome location, or high missingness. Missing values were imputed (impute.knn), Type-2 probe bias was corrected using Beta-Mixture Quantile normalization (BMIQ), and batch effects were adjusted using the ComBat function on M-values(Johnson et al. 2007; Teschendorff et al. 2013).

Serum metabolomics

For this study, we used serum metabolomics data from 3,037 individuals from the NSPT cohort (Lin et al. 2025), with the technical methods first reported in (Wu et al. 2021). Briefly, serum metabolomics was performed on a 600 MHz NMR spectrometer (Bruker Biospin), and data were quantified using Bruker's B.I.LISA™ and B.I.Quant-PS™ software. A total of 351 metabolite-related indicators were obtained through detection and calculation; we excluded indicators with a >20% missing rate. Finally, 336 metabolite-related indicators from 3,037 individuals were used for further analyses.

Genotype data processing

The genotype data for 3,513 NSPT samples were previously generated and described in (Peng et al. 2024). Briefly, samples were genotyped using the Illumina Infinium Global Screening Array. After stringent quality control using PLINK, the data were phased with SHAPEIT3 and imputed with IMPUTE2 using the 1000 Genomes Project phase 3 reference panel(Purcell et al. 2007; Howie et al. 2009; O'Connell et al. 2016). After post-imputation filtering, 8,603,582 high-quality SNPs were available for the analyses in this study.

Phenotype data processing

The physiological and blood biochemical phenotype data for the NSPT cohort were collected and described in a previous publication(Peng et al. 2025). Briefly, physiological measurements (e.g., height, weight, BMI, blood pressure) were taken on-site. Blood

biochemical phenotypes were obtained from serum samples, and a Toshiba TBA-40FR biochemical analyzer was used to measure 13 phenotypes, including ALT, AST, CHO, CREA, DBIL, GLU, HDL, IBIL, LDL, TBIL, TG, UA, and urea.

Statistical analysis

White method for detecting epigenetic drift-CpGs

To identify epigenetic drift-CpGs with heteroscedasticity related to age, we improved upon the two-step regression testing method based on White's heteroscedasticity test(White 1980).

Simulation benchmarking for heteroscedasticity testing of drift-CpGs

To evaluate the performance of existing heteroscedasticity testing methods in detecting epigenetic drift-CpGs, we simulated four different types of DNA methylation datasets:

Dataset 1 (Null model): To evaluate the Type I error rate, this dataset exhibited no heteroscedasticity or outliers. It consisted of 3,000 ages permuted from the real data and 10,000 randomly selected CpGs from our quality-controlled data.

Dataset 2 (Null model with outliers): To test for robustness, this dataset included outliers but no heteroscedasticity. It consisted of 3,000 ages permuted from the real data, with 10,000 simulated CpG values where the standard deviation was set to ten times the true standard deviation.

Dataset 3 (Linear heteroscedasticity): To test power for linear effects, this dataset simulated a linear relationship between CpG variance and age. It consisted of 3,000 ages

permuted from the real data and 10,000 simulated CpG values where the age regression coefficients for the variance of the residuals increased from 1×10^{-5} to 1×10^{-4}.

Dataset 4 (Non-linear heteroscedasticity): To test power for complex effects, this dataset simulated a non-linear relationship. For 3,000 ages permuted from the real data, the regression coefficient for CpG residual variance was set to -1.0×10^{-3} for ages ≤ 45, the variance was set to 1.0×10^{-2} for ages between 45 and 55, and the coefficient was set to 1.0×10^{-3} for ages > 55.

We then tested the Type I error and statistical power for four existing methods on each dataset:

Method A (DGLM): The Double Generalized Linear Model, using the dglm R package(Liu et al. 2023)

Method B (Likelihood Ratio Test): The heteroscedastic likelihood ratio test, using the gamlss R package(Bergstedt et al. 2022).

Method C (Breusch-Pagan Test): The Breusch-Pagan test for heteroscedasticity(Slieker et al. 2016).

Method D (White Test): The White test, as described in this study(White 1980).

Finally, we evaluated the performance of the four methods based on the false-positive rate (Dataset 1), the impact of outliers (Dataset 2), and the statistical power to detect linear (Dataset 3) and non-linear (Dataset 4) heteroscedasticity.

Epigenome-wide drift analysis: multi-scale functional characterization

To explore the correlation between DNA methylation variation and initial/terminal DNA methylation levels, we presented the changes in epigenetic drift and methylation levels. DNA methylation levels at significant drift-CpGs identified by our epigenome-wide drift analysis were compared between young (mean - 2 standard deviations) and old (mean + 2 standard deviations) NSPT populations. A scatter plot was generated using initial methylation levels from the younger group (x-axis) and terminal methylation levels from the older group (y-axis), with points colored according to drift direction (positive or negative). Additionally, heatmaps were constructed to visualize the density distributions of positive and negative drift-CpGs across predefined methylation intervals ([0–0.05], [0.05–0.1], [0.1–0.9], [0.9–0.95], [0.95–1]).

We applied the EpiDISH algorithm(Zheng et al. 2018) to estimate the proportions of major blood cell types-myeloid cells (monocytes and neutrophils) and lymphoid cells ($CD4^+$ T, $CD8^+$ T, NK, and B cells)-using DNA methylation profiles derived from blood plasma samples. For each cell type, individuals were stratified into three groups based on their estimated proportions: top 10% (high), bottom 10% (low), and middle 80% (intermediate) for illustrative purposes. To assess cell-type-specific contributions to methylation drift, we adapted the CellDMC framework (Zheng et al. 2018) to analyze significant drift-CpGs. For each CpG, we modeled the interaction between age and estimated cell-type proportion on a multiplicative scale, using the squared residual from a CpG ~ age regression as a quantitative measure of drift. The resulting *P*-values reflected the specificity of age-dependent

methylation drift across cell types.CpGs with Bonferroni-adjusted *P*-values < 0.05 were considered to show statistically significant cell-type-specific drift.

To elucidate the contribution of age-related methylation drift to inter-individual immune variation at single-cell resolution, we integrated population-scale epigenetic drift profiles with single-cell transcriptomic data from peripheral blood mononuclear cells (PBMCs) in the OneK1K cohort (number of samples = 982, number of cells=1,248,980)(Yazar et al. 2022). Specifically, we compared transcriptional dynamics between individuals at the extremes of the age spectrum, defined as the youngest 1% and oldest 1% of the cohort. Paired *t*-tests were used as a complementary approach to compare overall gene expression and noise distributions across age groups and drift categories. In addition, for each gene and for each immune cell type, we assessed age-associated changes in both transcriptional levels and transcriptional noise using the BASiCS algorithm(Vallejos et al. 2015). This method allowed us to simultaneously estimate changes in gene expression means and cell-to-cell variability between the young and old groups. Analyses were stratified by the direction of methylation drift (positive vs. negative drift-CpGs), enabling us to dissect whether specific drift patterns are linked to altered expression magnitude or variability within defined immune subpopulations.

We performed Transcription factor binding site (TFBS) enrichment analysis on drift-CpGs. For each CpG site, genomic sequences from two windows, 10 bp (±5 bp) and 30 bp (±15 bp), were extracted for analysis. TF enrichment was conducted using the TFmotifView web tool (Leporcq et al. 2020) (https://bardet.u-strasbg.fr/tfmotifview/), which compiles motif

information for 176 human transcription factors. Statistical significance was assessed using Bonferroni correction, with an adjusted *P*-value threshold of <0.05 considered statistically significant.

Epigenome-wide age-associated CpG analysis

To identify the age-associated CpGs, termed here as clock-CpGs, we used a linear model to perform epigenome wide association analysis based on 469,061 CpGs in the NSPT cohort with the same starting amount as EWDS. *P* value smaller than 1×10^{-7} (Bonferroni $P < 0.05$) were considered as epigenome-wide significant. Covariates included gender, BMI, cell composition, experiment batch, the first 5 genetic principal components and the first 5 epigenetic principal components. Genomic principal components (genomic PCs) were calculated using PLINK 1.9 based on all genome-wide SNPs. For methylation principal components (methylation PCs), we applied the prcomp function in R to the β values of 810,000 CpG sites across the genome.

Biological annotations

To provide biological annotation of the identified methylation sites, the CpGs were mapped by referring to the manufacturer's manifest files (GRCh37 hg19 build). We aligned data to GRCh37 (hg19) because our Illumina methylation array probes are predominantly annotated to this assembly. This also ensured consistency with vast public datasets. Given that most gene associations are conserved across genome builds and our epigenetic drift analyses focus on well-characterized genomic regions, we do not expect the use of a more recent assembly (e.g., GRCh38) to significantly impact our biological conclusions. The genomic annotations

196 contained: Enhancer (in FANTOM5 project defined enhancer regions), TSS1500 (200-1500
197 bases upstream of the TSS), TSS200 (0-200 bases upstream of the transcriptional start site),
198 UTR5 (within the 5' untranslated regions), 1stExon (the first exon), ExonBnd (within 20
199 bases of an exon boundary, i.e. the start or end of an exon), Body (gene body) and UTR3
200 (within a 3' untranslated region), Promoter (the union of TSS1500, TS200, 1stExon and 5'
201 UTR). The CpG island annotations included: N_Shelf (upstream 2-4 kb from CpG islands),
202 N_Shore (upstream 0-2 kb from CpG islands), Island, S_Shore (downstream 0-2 kb from
203 CpG islands) and S_Shelf (downstream 2-4 kb from CpG islands). Odds ratio was calculated
204 as follows:

205 $$Odds\ Ratio = \frac{N_f/(N_{drift} - N_f)}{N_{whole\_f}/(N - N_{whole\_f})}$$

206 N is the total CpG number, N_{whole_f} is the CpG in N which were located in the
207 functional region, N_{drift} is the drift-CpG number, N_f is the CpG in N_{drift} which were
208 located in the functional region.

209 To explore the functional differences of different types of drift and clocks, we conducted
210 relative enrichment analysis of chromosome states and gene regions separately for positive
211 and negative drift, as well as positive and negative clocks. Finally, we assessed the
212 significance using a hypergeometric test with a significance threshold of 0.05.

213 **Replication analysis**

214 Drift-CpGs significant in the discovery analysis (Bonferroni threshold $P < 1\times10^{-7}$) were
215 followed up with a replication analysis in CAS data based on White method. Next, to examine

the reliability of drift-CpGs in other ancestral populations, we extracted methylation sites from European-derived methylation data that significantly overlapped with CAS validation. Furthermore, we used the White method to validate the drift-CpGs using the GSE40279 dataset, which includes a mixed population of 426 Caucasian and 230 Hispanic individuals, assessed with a 450K beadchip, and with an age range of 19-101(Hannum et al. 2013).

In the replication analysis of the longitudinal Changfeng population, 410,440 CpG sites were retained that matched with NSPT. The delta beta between the two time points was calculated for each CpG site, and then the average delta beta at the individual level was computed. Five samples were excluded, which had individual mean delta beta values exceeding 3 standard deviations from the mean, resulting in 402 remaining samples used for further analysis. The CpG drift value between the two stages was calculated for each CpG site using the following formula:

$$CpG_{drift\ i,n,s} = (CpG_{i,n,s} - CpG_{NSPT\ i})^2$$

Here, i refers to CpG site, n refers to sample, and s refers to stage. A paired *t*-test was performed on the CpG-drift values for the two stages and a significance threshold of $P < 0.05$ was used.

Finally, we investigated the stability of drift in a twin cohort using the GSE61496 dataset, which comprised 150 pairs of MZ twins assessed with a 450K beadchip, with 78 pairs being male and 72 pairs being female twins, and with an age range of 30-74 (Tan et al. 2014). We extracted methylation sites from the twin methylation data that significantly overlapped with CAS validation and then fitted a linear regression model to the absolute difference in age

and twin pair values. Drift-CpGs with a $P < 0.05$ and an effect direction consistent with the discovery analysis were considered successful replications.

Construction of epigenetic drift score (EDS)

To construct an EDS that quantifies an individual's level of positive epigenetic drift, we began by selecting drift-CpGs as representatives of the overall epigenetic drift status in an individual. First, we selected the NSPT-significant drift-CpGs ($P < 1\times10^{-7}$) that are also CAS-replicated drift-CpGs ($P < 5\times10^{-2}$) and Hannum-replicated drift-CpGs ($P < 5\times10^{-2}$) to ensure that all selected drift-CpGs are robustly replicated. Then, we calculated the Fisher combined *P*-values for the significantly associated drift-CpGs from these three cohorts and removed all CpGs within a 500-kilobase pair distance of the region's most significant drift-CpG in any genomic region, resulting in a set of 2,069 independent and informative drift-CpGs. Subsequently, we computed the variability of the chosen drift-CpGs and quantified an individual's drift status by aggregating the age-correlated weighted variances. The score for each drift site was computed as $s_{ij} = (\beta_{ij} - \bar{\beta}_j)^2/SD_j$, where s_{ij} denotes the drift magnitude for individual *i* at site *j*, β_{ij} is the methylation level for individual *i* at site *j*, $\bar{\beta}_j$ is the mean methylation level at site *j*, and SD_j is the standard deviation of methylation at site *j*. A non-negative least squares regression between each site's drift score s_{ij} and the age of the individual y_i was then performed, $y_i = \delta_{0j} + \delta_{1j}s_{ij}$, where δ_{0j} is the intercept term and δ_{1j} is the regression coefficient reflecting the correlation between drift score and age. This step of non-negative least squares regression ultimately selected 204 CpG sites with non-zero coefficients for constructing the positive epigenetic drift score. The overall positive epigenetic

drift score s_i for individual *i* was calculated by summing across all *k*=204 drift sites, weighted by the regression coefficient, $s_i = \sum_{j=1}^{k} \delta_{1j} s_{ij}$. Here the weighting factors derived from the regression on the NSPT and Hannum cohorts are used as a standard reference for calculating positive epigenetic drift score in other cohorts without the need for re-estimation. For normalization, we adapted the range normalization method to make positive epigenetic drift score comparable across populations that were not part of the initial NSPT and Hannum cohorts. We linearly transformed the individual drift score s_i to a range between 0 and 1. This was done using the NSPT and Hannum cohorts as reference populations to anchor the minimum and maximum possible drift scores, denoted as $min(s_i)$ and $max(s_i)$, projected at ages 0 and 120 years respectively. The normalized positive epigenetic drift score (EDS_POS) S_i for individual *i* is calculated as $S_i = \frac{s_i - min(s_i)}{max(s_i) - min(s_i)}$.

For individual's level of negative epigenetic drift, we directly used the drift scores of all significant drift-CpGs from NSPT and construct a non-negative least squares regression model. Ultimately, we obtained 81 negative drift sites with non-zero coefficients for the construction of the negative epigenetic drift score (EDS_NEG), and the scores were range standardized to a scale of 0-1 for ages 0-120.

We implemented an entropy-based approach adapted from (Scherer et al. 2020) to measure individual-level DNA methylation variability using Illumina EPIC array-derived β-values. For each participant in the NSPT cohort, we computed genome-wide entropy separately for positive and negative drift CpGs, using the Shannon entropy formula: $H = -\Sigma[p*\log_2(p+1\times10^{-4})]$, where p represents the methylation β-value at each CpG site. We then

evaluated the concordance between these individual entropy measures and population-level epigenetic drift scores (EDS_POS and EDS_NEG) through Pearson's correlation analysis. In the longitudinal Changfeng cohort, we assessed temporal changes in entropy measures between baseline and 4-year follow-up using two-tailed paired *t*-tests, with statistical significance defined as $P < 0.05$.

Assessment of the association between EDS and age

To assess the association between EDS and age, we first calculated the correlation between EDS and age in the NSPT and CAS cohorts, and evaluated the differences in EDS distribution among different gender groups. Next, to quantify the contribution of selected drift-CpGs to the EDS, we calculated the correlation between the drift score and age as the number of positive drift-CpGs increased from 1 to 204 and negative drift-CpGs increased from 1 to 81, respectively. We then displayed the changes in the cumulative curve using R, with a step size of 50 and 50 repetitions at each step..

To measure the association between EDS and published methylation-based age indicators, we calculated the epigenetic age based on the Horvath and Hannum clocks (first-generation clocks), Levine's phenotypic age (second-generation clock), and Dunedin's aging rate (third-generation clock) using NSPT and CAS samples. We evaluated the Pearson's correlation before and after adjusting for chronological age, with a significance level of $P < 0.05$. Finally, we displayed the results in a heatmap using the R package corrplot.

Association assessment of EDS and metabolome

To examine the impact of epigenetic drift on lipid metabolism, we conducted an association analysis between EDS and lipidomic data in the NSPT cohort, which included both DNA methylation data and lipidomic profiles. Based on the composition and concentration indicators of 336 NMR-detected lipoprotein subfractions (including 176 measured values and 175 derived values), we performed linear regression analyses to examine the associations between metabolic indicators and EDS, while adjusting for covariates such as BMI, age, gender, and population. To determine statistical significance, we used FDR-adjusted $P < 0.05$ as the threshold. To compare the associations of the epigenetic drift scores and other methylation indicators with metabolism, we separately assessed the significance of the associations between the Horvath and Hannum clocks (first-generation clocks), Levine's phenotypic age (second-generation clock), and Dunedin's aging rate (third-generation clock) with metabolic indicators.

Finally, we visualized the effect sizes of significant metabolic traits through a forest plot and displayed the correlations among metabolic traits using a heatmap. These visualizations were generated using the R package forestplot.

GWAS analysis of EDS

To identify potential genes associated with epigenetic drift, we performed a genome-wide association analysis of EDS using the NSPT samples, which had both DNA methylation data and genomic data available. We employed linear regression models, implemented in PLINK (Purcell et al. 2007), to examine the associations between EDS and SNPs. The models were

adjusted for covariates such as age, gender, and the top 10 principal components of the genomic data. The significance threshold is $P < 5\times10^{-8}$. Additionally, we utilized the GCTA(Yang et al. 2011) software to estimate the heritability of EDS, providing insights into the proportion of phenotypic variance that can be attributed to genetic factors. Finally, we analyzed chromatin state changes during aging using Integrative Genomics Viewer (IGV), leveraging hMSC data from GSE156409 (McCauley et al. 2021). The young group comprised early-passage cells at population doubling (PD)12, while the old group consisted of late-passage PD32 cells.

Published software

We utilized publicly available software, which can be requested using the following URLs: R (V4.4.0, https://cran.r-project.org/)(R Core Team 2024); R package ggplot2 for visualization (V3.5.1, https://cran.r-project.org/web/packages/ggplot2/index.html); R package diptest for unimodality test (V0.77-1, https://cran.r-project.org/web/packages/diptest/index.html); R package missMethyl for GO and KEGG pathway enrichment analyses (V3.13, https://bioconductor.org/packages/3.13/bioc/html/missMethyl.html); R package poolr for stringent Tippett test (V1.1-1, https://cran.r-project.org/web/packages/poolr/index.html); R package corrplot for correlation visualization (V0.94, https://cran.r-project.org/web/packages/corrplot/index.html); R package forestplot for effect sizes visualization (V3.1.3, https://cran.r-project.org/web/packages/forestplot/index.html); SHAPEIT3 for phasing (SHAPEIT3, https://jmarchini.org/shapeit3); IMPUTE2 for imputation (IMPUTE version 2, https://mathgen.stats.ox.ac.uk/impute/impute_v2.html);

PLINK for SNP data-processing (PLINK2.0, https://www.cog-genomics.org/plink/2.0);

GCTA for heritability calculation (V1.93.2 beta, http://cnsgenomics.com/software/gcta). IGV

for interactive genome visualization (IGV, https://igv.org/)

Supplemental Figures

Supplemental Figure S1

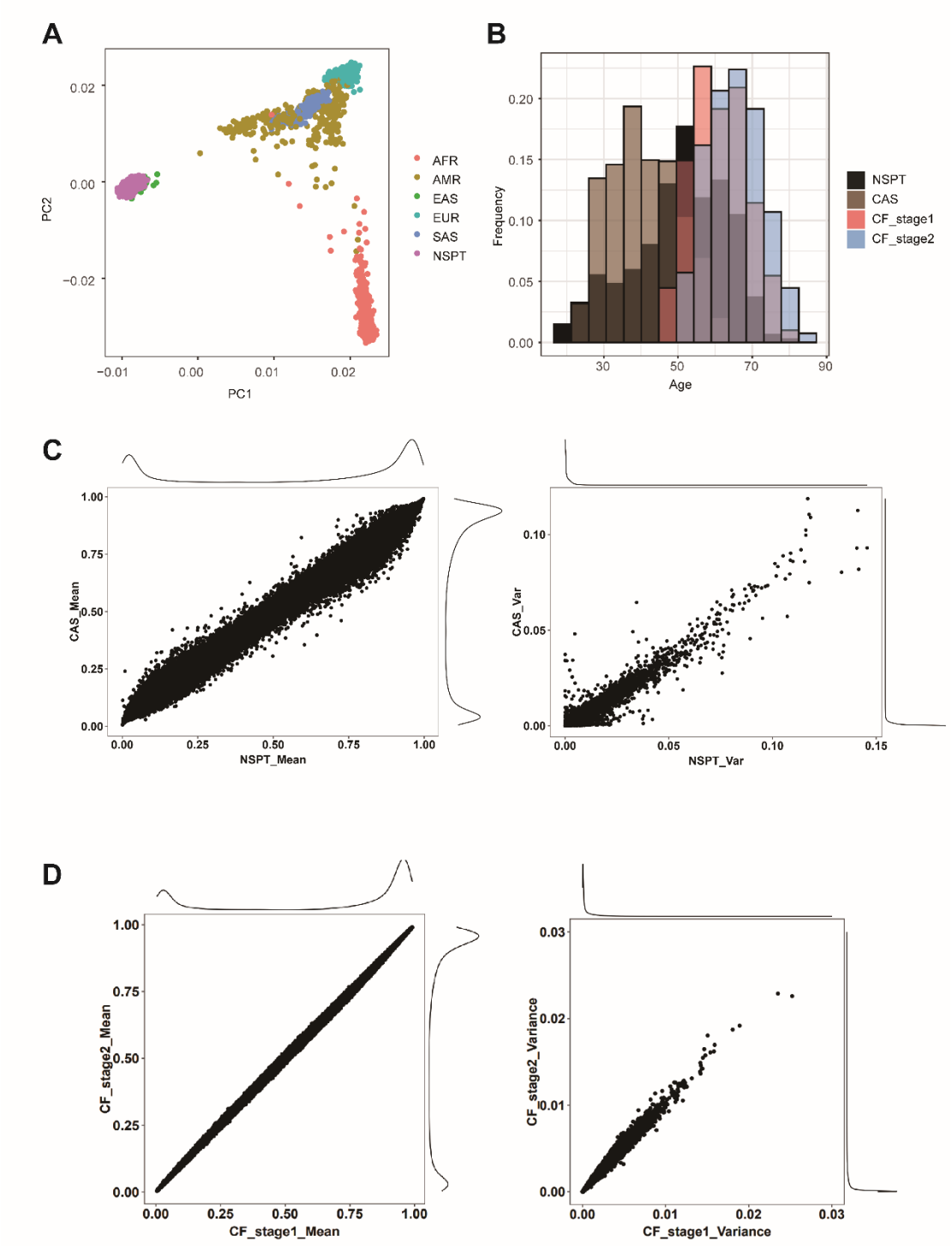

Figure S1. Quality control of the population distributions and DNA methylation data. **A**, The top genotype principal components (PC1 and PC2) exhibit that NSPT samples represents the genetic characteristics of East Asian populations. **B**, Histogram of age distribution for NSPT, CAS, and Changfeng (CF) samples. **C**, The scatter plot demonstrates the consistency between NSPT and CAS in terms of the mean and variance of DNA methylation of CpGs. **D**, The scatter plot illustrates the consistency of mean and variance of DNA methylation between the Changfeng (CF) baseline and follow-up.

Supplemental Figure S2

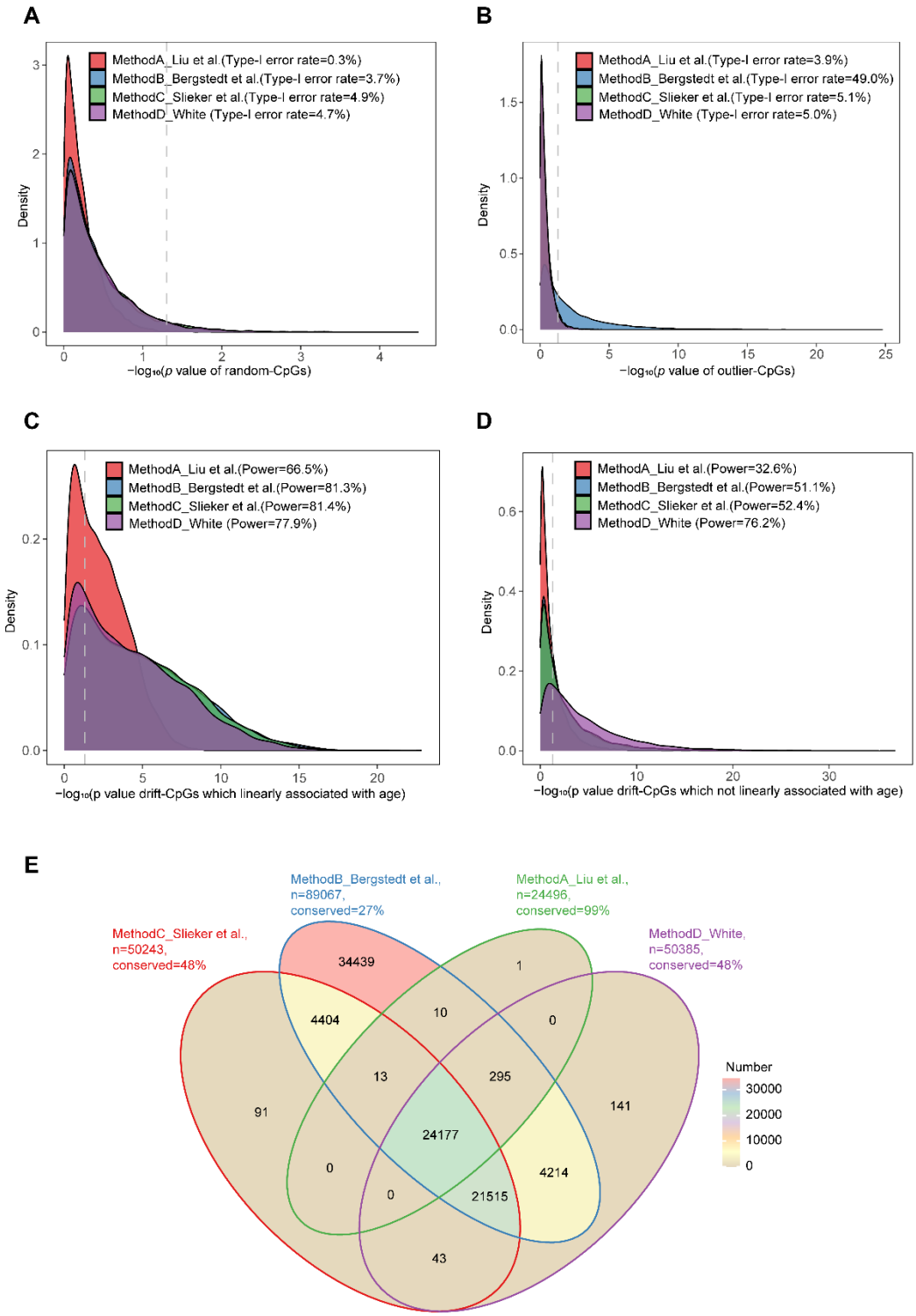

Figure S2. Benchmarking of epigenetic drift statistical methods. **A**, Method A (Liu et al.) exhibits an overly conservative type I error rate at the significance threshold of 0.05 under the

null hypothesis. **B**, Method B (Bergstedt et al.) exhibits an elevated type I error rate under the null hypothesis when artificial outliers are introduced. **C**, Method A (Liu et al.) shows the lowest power in a scenario where CpG variance is linearly correlated with the square of age. **D**, Method D (White method) shows the highest power in a scenario with a non-linear relationship between CpG variance and age. **E**, Method D identifies the most epigenetic drift-CpGs in real DNA methylation data.

Supplemental Figure S3

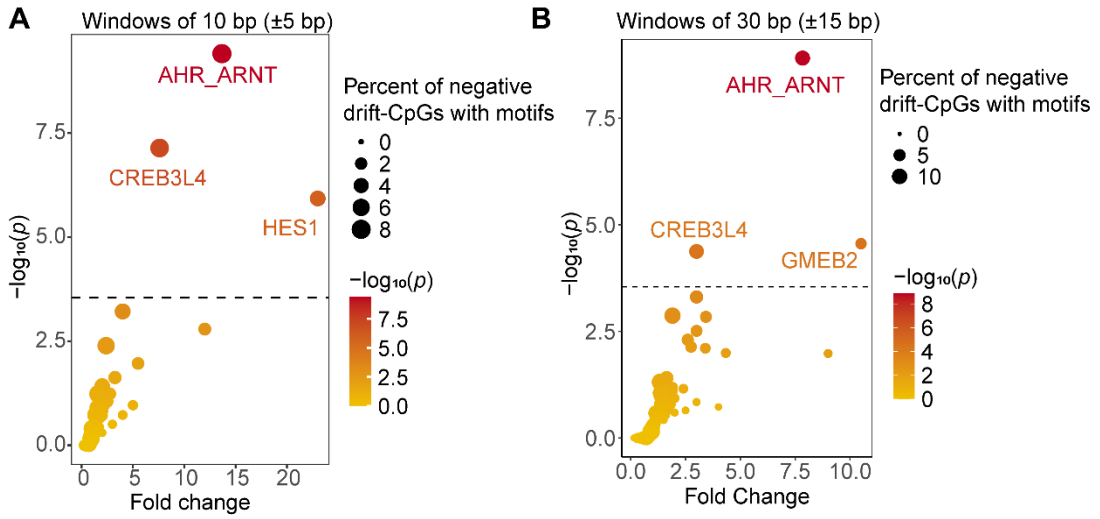

Figure S3. Enrichment of transcription factor binding motifs around negative drift-CpGs. Enrichment of transcription factor binding motifs around negative drift-CpGs. Volcano plots show motif enrichment in genomic regions flanking negative drift-CpGs, analyzed using (A) 10 bp windows (±5 bp) and (B) 30 bp windows (±15 bp). Each point represents a unique transcription factor motif. The x-axis shows the fold change of the motif, and the y-axis indicates its statistical significance ($-\log_{10}(P)$). The dashed line marks the Bonferroni-corrected significance threshold ($P = 2.8 \times 10^{-4}$). The color of each point corresponds to its significance, while its size reflects the percentage of negative drift-CpGs that contain the motif.

Supplemental Figure S4

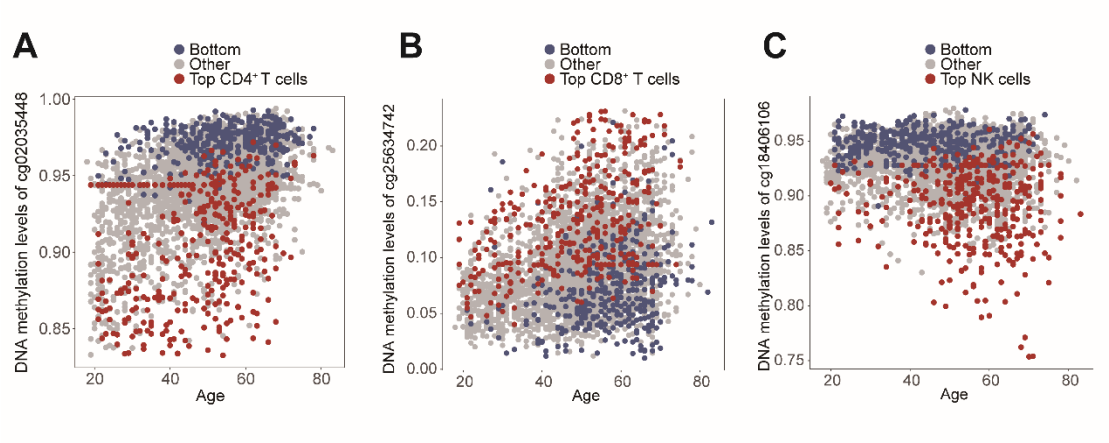

Figure S4. Cell type-specific DNA methylation changes at epigenetic drift-CpGs during aging. A, DNA Methylation levels of $CD4^+$ T cell-specific negative drift cg02035448 drifting with age. **B,** DNA Methylation levels of $CD8^+$ T cell-specific positive drift cg25634742 drifting with age. **C,** DNA Methylation levels of NK cell-specific positive drift cg18406106 drifting with age.

Supplemental Figure S5

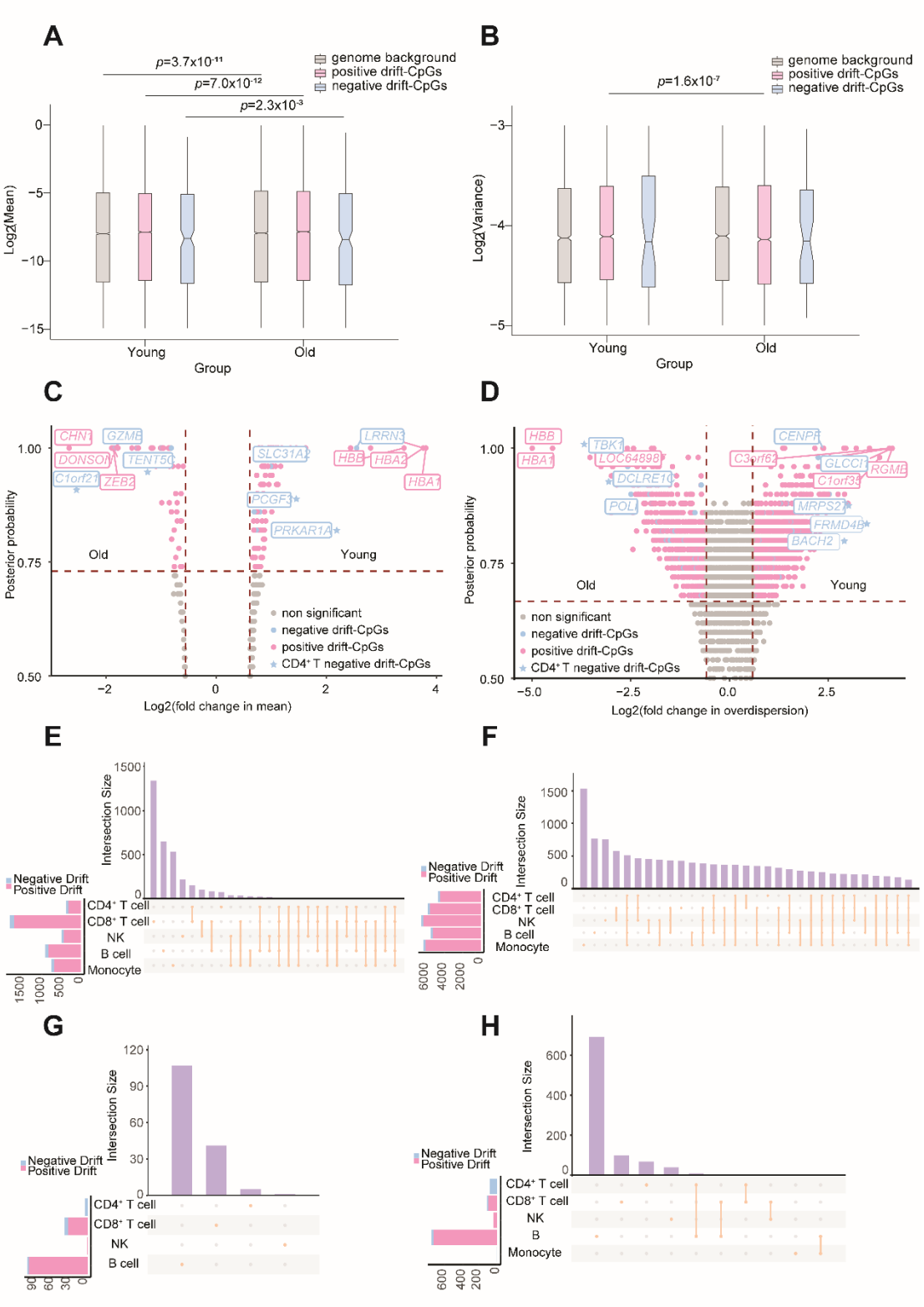

Figure S5. Association between epigenetic drift and transcriptional alterations across immune cell types during aging. **A**, Mean expression changes linked to epigenetic drift with

392 age. **B**, Transcriptional noise changes linked to epigenetic drift with age. **C-D,** BASiCS-
393 identified transcriptional changes in $CD4^+$ T cells for genes near drift-CpGs: mean expression
394 (C) and overdispersion (D). The colors of CpG sites are divided based on the direction of
395 drift-CpGs. Genes annotated by drift-CpGs are labelled by text. The asterisk indicates the
396 epigenetic drift that is dependent on the $CD4^+$ T cell type component. **E-F**, Upset plots
397 showing cell-specific transcriptional mean (E) and noise (F) changes of drift-associated genes
398 across lymphoid lineages ($CD4^+$ T, $CD8^+$ T, NK, B cells) and monocytes. **G-H**, Cell type-
399 specific mean (G) and noise (H) changes for lymphoid populations.
400
401

Supplemental Figure S6

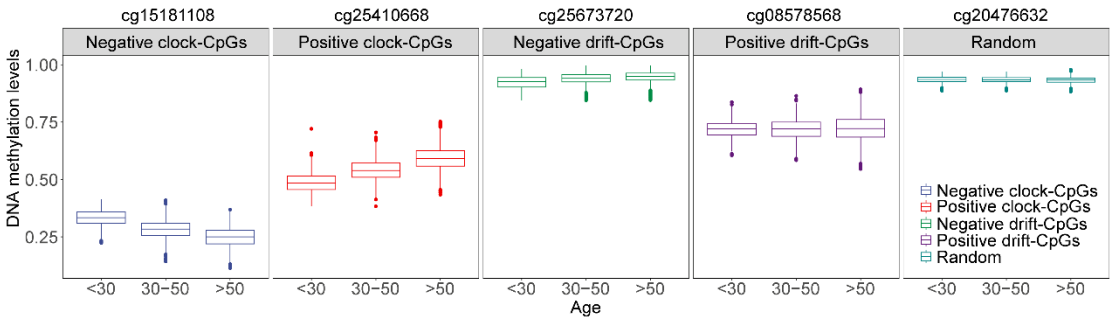

Figure S6. Examples of DNA methylation changes at epigenetic clock- and drift-CpGs during aging.

Supplemental Figure S7

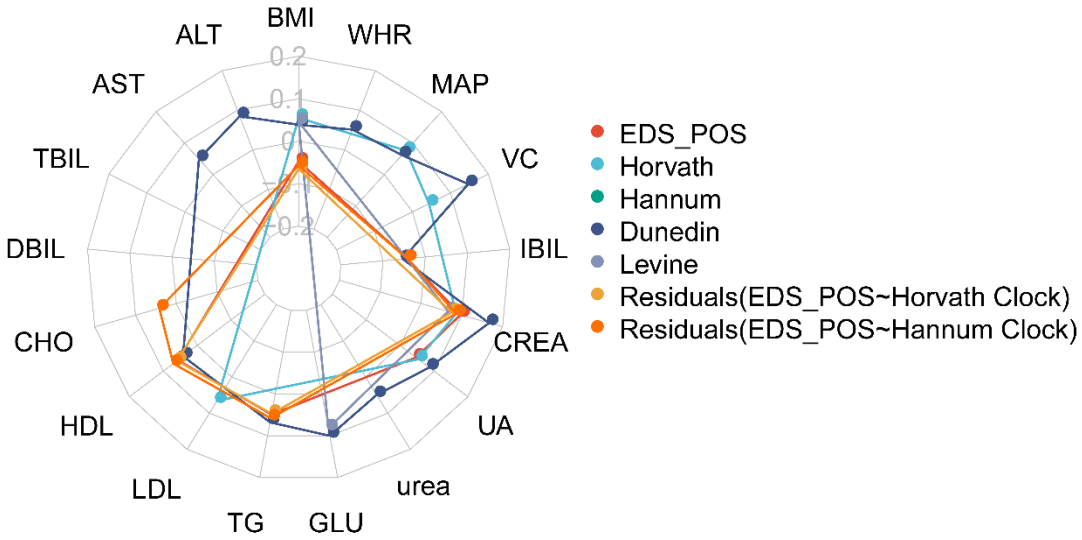

Figure S7. Correlations between age-related epigenetic indicators and blood biochemical phenotypes. Residuals (EDS_POS~Horvath Clock) means that the correlation between positive EDS and blood biochemical phenotypes was additionally adjusted for the effect of Horvath aging score. Residuals (EDS_POS~Hannum Clock) means that the correlation between positive EDS and blood biochemical phenotypes was additionally adjusted for the effect of Hannum aging score.

Supplemental Figure S8

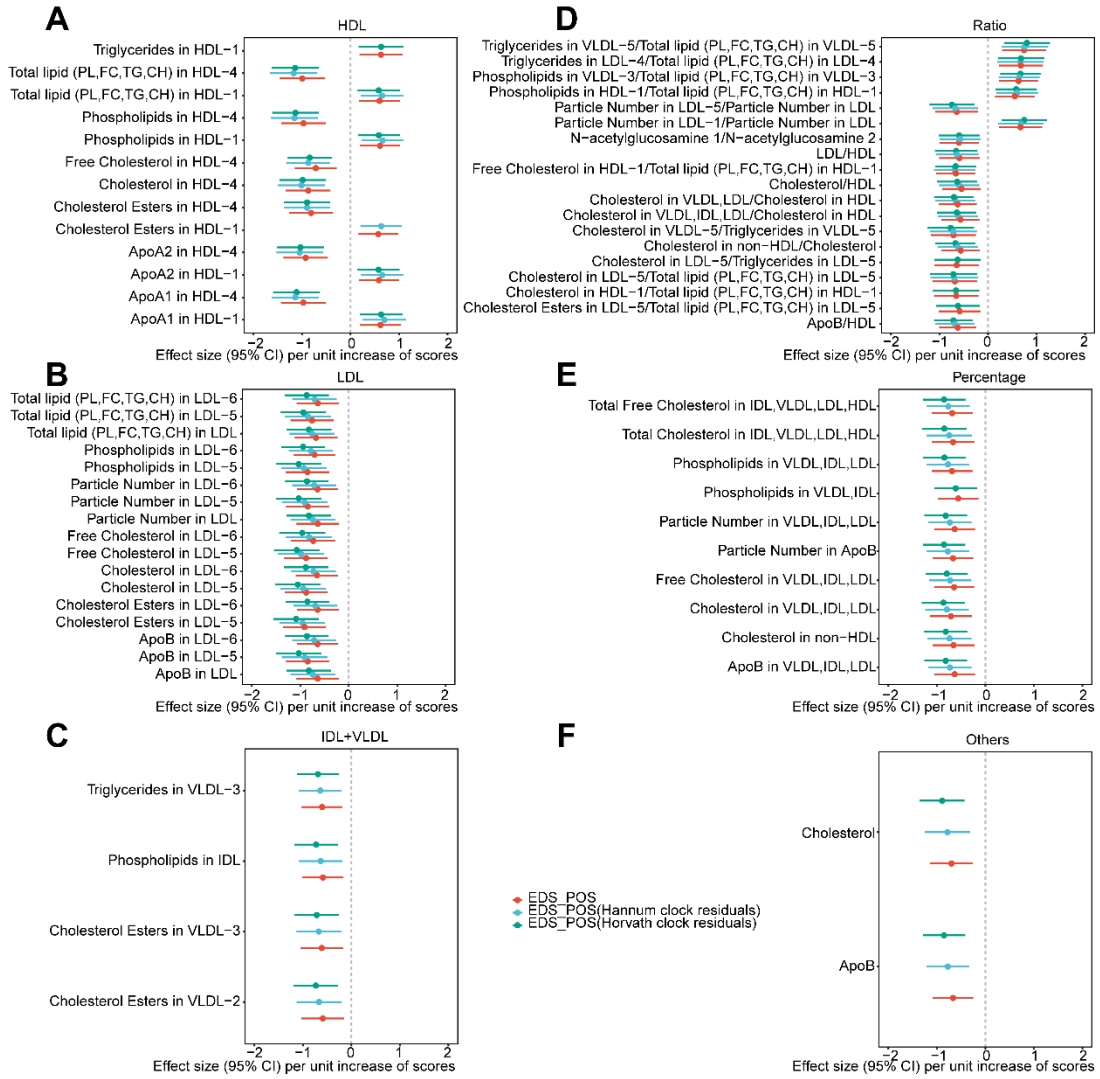

Figure S8. Associations of EDS_POS with lipid metabolism, with and without epigenetic clock adjustment. Forest plots display effect sizes (with 95% confidence intervals) per unit increase of relevant scores on various lipid metrics. Associations shown are significant at FDR $P < 0.05$. Three models are presented: Unadjusted EDS_POS (red), EDS_POS adjusted for Hannum clock residuals (blue), and EDS_POS adjusted for Horvath clock residuals (green). **A**, Associations with HDL-related traits. **B**, Associations with LDL-related traits. C**,** Associations with IDL- and VLDL-related traits. **D**, Associations with lipid ratios. **E**,

426 Associations with lipid component percentages. **F**, Associations with other small metabolites

427 and apolipoproteins.

Supplemental Tables

Supplemental Table S1

Table S1. Characteristics of the study populations (Supplemental_Table_S1.xlsx).

Supplemental Table S2

Table S2. Epigenetic clock effect of drift-CpGs (Supplemental_Table_S2.xlsx).

Supplemental Table S3

Table S3. DNA methylation drift-CpGs discovered in NSPT and replicated in CAS (Supplemental_Table_S3.xlsx).

Supplemental Table S4

Table S4. Drift-CpGs list composing EDS_POS (Supplemental_Table_S4.xlsx).

Supplemental Table S5

Table S5. Drift-CpGs list composing EDS_NEG (Supplemental_Table_S5.xlsx).

Supplemental Table S6

Table S6. Significant associations between epigenetic scores and lipid metabolism (Supplemental_Table_S6.xlsx).

References

Aryee MJ, Jaffe AE, Corrada-Bravo H, Ladd-Acosta C, Feinberg AP, Hansen KD, Irizarry RA. 2014. Minfi: a flexible and comprehensive Bioconductor package for the analysis of Infinium DNA methylation microarrays. *Bioinformatics* **30**: 1363-1369.

Bergstedt J, Azzou SAK, Tsuo K, Jaquaniello A, Urrutia A, Rotival M, Lin DTS, MacIsaac JL, Kobor MS, Albert ML et al. 2022. The immune factors driving DNA methylation variation in human blood. *Nat Commun* **13**: 5895.

Gao X, Hofman A, Hu Y, Lin H, Zhu C, Jeekel J, Jin X, Wang J, Gao J, Yin Y et al. 2010. The Shanghai Changfeng Study: a community-based prospective cohort study of chronic diseases among middle-aged and elderly: objectives and design. *Eur J Epidemiol* **25**: 885-893.

Hannum G, Guinney J, Zhao L, Zhang L, Hughes G, Sadda S, Klotzle B, Bibikova M, Fan JB, Gao Y et al. 2013. Genome-wide methylation profiles reveal quantitative views of human aging rates. *Mol Cell* **49**: 359-367.

Howie BN, Donnelly P, Marchini J. 2009. A flexible and accurate genotype imputation method for the next generation of genome-wide association studies. *PLoS Genet* **5**: e1000529.

Johnson WE, Li C, Rabinovic A. 2007. Adjusting batch effects in microarray expression data using empirical Bayes methods. *Biostatistics* **8**: 118-127.

Leporcq C, Spill Y, Balaramane D, Toussaint C, Weber M, Bardet AF. 2020. TFmotifView: a webserver for the visualization of transcription factor motifs in genomic regions. *Nucleic Acids Res* **48**: W208-w217.

Li W, Xia M, Zeng H, Lin H, Teschendorff AE, Gao X, Wang S. 2024. Longitudinal analysis of epigenome-wide DNA methylation reveals novel loci associated with BMI change in East Asians. *Clin Epigenetics* **16**: 70.

Lin C, Xia M, Dai Y, Huang Q, Sun Z, Zhang G, Luo R, Peng Q, Li J, Wang X et al. 2025. Cross-ancestry analyses of Chinese and European populations reveal insights into the genetic architecture and disease implication of metabolites. *Cell Genomics* **5**.

Liu Y, Sinke L, Jonkman TH, Slieker RC, van Zwet EW, Daxinger L, Heijmans BT. 2023. The inactive X chromosome accumulates widespread epigenetic variability with age. *Clin Epigenetics* **15**: 135.

McCauley BS, Sun L, Yu R, Lee M, Liu H, Leeman DS, Huang Y, Webb AE, Dang W. 2021. Altered Chromatin States Drive Cryptic Transcription in Aging Mammalian Stem Cells. *Nat Aging* **1**: 684-697.

Morris TJ, Butcher LM, Feber A, Teschendorff AE, Chakravarthy AR, Wojdacz TK, Beck S. 2014. ChAMP: 450k Chip Analysis Methylation Pipeline. *Bioinformatics* **30**: 428-430.

O'Connell J, Sharp K, Shrine N, Wain L, Hall I, Tobin M, Zagury JF, Delaneau O, Marchini J. 2016. Haplotype estimation for biobank-scale data sets. *Nat Genet* **48**: 817-820.

Peng Q, Cheung YK, Liu Y, Wang Y, Tan J, Yang Y, Wang J, Han J-DJ, Jin L, Liu F et al. 2025. 3D facial imaging: a novel approach for metabolic abnormalities risk profiling. *Science China Life Sciences* **68**: 1786-1800.

Peng Q, Liu X, Li W, Jing H, Li J, Gao X, Luo Q, Breeze CE, Pan S, Zheng Q et al. 2024. Analysis of blood methylation quantitative trait loci in East Asians reveals ancestry-specific impacts on complex traits. *Nature Genetics* **56**: 846-860.

Purcell S, Neale B, Todd-Brown K, Thomas L, Ferreira MA, Bender D, Maller J, Sklar P, de Bakker PI, Daly MJ et al. 2007. PLINK: a tool set for whole-genome association and population-based linkage analyses. *Am J Hum Genet* **81**: 559-575.

R Core Team. 2024. R: A Language and Environment for Statistical Computing. R Foundation for Statistical Computing.

Scherer M, Nebel A, Franke A, Walter J, Lengauer T, Bock C, Müller F, List M. 2020. Quantitative comparison of within-sample heterogeneity scores for DNA methylation data. *Nucleic Acids Research* **48**: e46-e46.

Slieker RC, van Iterson M, Luijk R, Beekman M, Zhernakova DV, Moed MH, Mei H, van Galen M, Deelen P, Bonder MJ et al. 2016. Age-related accrual of methylomic variability is linked to fundamental ageing mechanisms. *Genome Biol* **17**: 191.

Tan Q, Frost M, Heijmans BT, von Bornemann Hjelmborg J, Tobi EW, Christensen K, Christiansen L. 2014. Epigenetic signature of birth weight discordance in adult twins. *BMC Genomics* **15**: 1062.

Teschendorff AE, Marabita F, Lechner M, Bartlett T, Tegner J, Gomez-Cabrero D, Beck S. 2013. A beta-mixture quantile normalization method for correcting probe design bias in Illumina Infinium 450 k DNA methylation data. *Bioinformatics* **29**: 189-196.

Vallejos CA, Marioni JC, Richardson S. 2015. BASiCS: Bayesian Analysis of Single-Cell Sequencing Data. *PLoS Comput Biol* **11**: e1004333.

White H. 1980. A Heteroskedasticity-Consistent Covariance Matrix Estimator and a Direct Test for Heteroskedasticity. *Econometrica* **48**: 817-838.

Wu Q, Huang QX, Zeng HL, Ma S, Lin HD, Xia MF, Tang HR, Gao X. 2021. Prediction of Metabolic Disorders Using NMR-Based Metabolomics: The Shanghai Changfeng Study. *Phenomics* **1**: 186-198.

Yang J, Lee SH, Goddard ME, Visscher PM. 2011. GCTA: a tool for genome-wide complex trait analysis. *Am J Hum Genet* **88**: 76-82.

Yazar S, Alquicira-Hernandez J, Wing K, Senabouth A, Gordon MG, Andersen S, Lu Q, Rowson A, Taylor TRP, Clarke L et al. 2022. Single-cell eQTL mapping identifies cell type-specific genetic control of autoimmune disease. *Science* **376**: eabf3041.

Zheng SC, Breeze CE, Beck S, Teschendorff AE. 2018. Identification of differentially methylated cell types in epigenome-wide association studies. *Nat Methods* **15**: 1059-1066.